Chemical Solution Deposition of $(Pb_{1-x}Ca_x)TiO_3$ thin films with x~0.5 as new dielectrics for tunable components and dynamic random access memories

M.L.Calzada♠, I.Bretos, R.Jiménez, J.Ricote and J.Mendiola

Inst. Ciencia de Materiales de Madrid. CSIC. Cantoblanco. 28049-Madrid. Spain.

J.García-López and M.A.Respaldiza

Dpt. Física Atómica, Nuclear y Molecular. Univ.Sevilla. 41080 – Sevilla, and Centro Nacional de Aceleradores (CNA). Parque Tecnológico Cartuja 93. 41092- Sevilla. Spain.

Abstract. Calcium lead titanate ($(Pb,Ca)TiO_3$) thin films, with calcium contents of ~50 at%, have been prepared by chemical solution deposition (CSD). Different synthetic sol-gel methods have been used for the preparation of the precursor solutions. 1,3-propanediol, $OH(CH_2)_3OH$, and water, H_2O, were used as solvents. Lead (II) acetate trihydrate, $Pb(OCOCH_3)_2.3H_2O$, and titanium di-isopropoxide bis(acetylacetonate), $Ti(OC_3H_7)_2(CH_3COCHCOCH_3)_2$, were used as reagents of lead and titanium, respectively. Calcium was incorporated to the solutions as calcium acetate hydrate, $Ca(OCOCH_3)_2.xH_2O$, or as calcium acetylacetonate hydrate, $Ca(CH_3COCHCOCH_3)_2.xH_2O$. Only the use of calcium acetate led to precipitate-free solutions. Pb(II)-Ti(IV)-Ca(II) sols were obtained when calcium acetate was refluxed with the lead and titanium reagents in a diol-water solvent. These sols led to films with a homogeneous compositional profile. Solutions obtained by mixing a water solution of calcium acetate with a Pb(II)-Ti(IV) sol led to films with a heterogeneous compositional profile in which an interface between the film and the Pt bottom electrode is formed. The films derived from the Pb(II)-Ti(IV)-Ca(II) sols have values of dielectric constant at room temperature of ~500, which together with their low leakage currents, low dielectric losses and tunability make these films promising for the DRAM and tunable devices.

♠ Author to whom correspondence should be addressed. Email: lcalzada@icmm.csic.es

1. Introduction

A series of ferroelectric compositions based on incipient ferroelectrics such as strontium titanate ($SrTiO_3$, ST) or calcium titanate ($CaTiO_3$, CT) have attracted during the last years a great deal of attention for microelectronic applications.

Substitution of Sr^{2+} by Ba^{2+} in ST leads to ferroelectric barium strontium titanate ($(Ba,Sr)TiO_3$, BST) materials. Bulk materials of these compositions have high dielectric constants, ε', low dielectric losses, tan δ, and non-linear behaviour. These are properties required in dynamic random access memories (DRAM) and tunable devices.[1,2] Therefore, BST is being investigated as a candidate to replace silicon dioxide (SiO_2) in these applications[1] in the near future. However, these materials in thin film form have shown inferior properties related with a large decrease of the dielectric constant due to the effect on it of an interfacial capacitance mainly coming from grain boundaries or dead layers. Values of ε' over 1000 (~1500) and low tan δ (~0.002) have been obtained in BST films, only when they are prepared at high temperatures (~1273 K) onto non-silicon substrates ((100) strontium titanate and (100) lanthanum aluminate)[3]. But, the key motivation of the microelectronic devices above indicated is the integration of the ferroelectric thin film with silicon. This demands the use of low temperatures (<1000 K). BST thin films on silicon substrates[4-6] have much worse values of ε', and tan δ (ε'~600 and tan δ~0.02).

In the search of other high dielectric constant materials which could show improved properties for these applications, J.Hao *et al.*[7] have reported the tunable properties of 1000 nm CT thick films. A dielectric constant of ε'~150 was measured at room temperature, maximum dielectric losses of tan δ~0.003 were obtained and a tunability of ~3% was calculated using the following equation:

$$\text{tunability} = (\varepsilon'(0) - \varepsilon'(E_{max})) / \varepsilon'(0) \qquad \text{eq.(1)}$$

where $\varepsilon'(0)$ is the dielectric constant at 0 V and $\varepsilon'(E_{max})$ is the dielectric constant at the maximum applied field (E_{max} here is 300 KV.cm^{-1}).

Neither dielectric constant nor tunability are too high in CT films, however the very low losses make that the figure of merit of these films for tunable applications is appropriate. Figure of merit was calculated as follows:

$$\text{Figure of merit} = \text{tunability} / \tan\delta \qquad \text{eq.(2)}$$

Substitution of Ca^{2+} by Pb^{2+} in CT leads to ferroelectric calcium lead titanate ($(Pb,Ca)TiO_3$, PCT) materials.[8] PCT bulk ceramics with Ca^{2+} contents below ~30 at% have been extensively studied, and their properties exploited in medical ultrasonic diagnostic or non-destructive evaluation.[9-13] Recently, a resurgent interest on PCT ceramics has appeared, especially for Ca^{2+} contents close to 50 at%.[14-17] Here, studies have been focused on crystal structure. Thus, a superstructure due to the tilting of oxygen octahedral has been proposed for bulk ceramics of this composition. [14-17] It has also been recently reported the existence in these ceramics of a morphotropic phase boundary for Ca^{2+} contents close to 50 at%, where tetragonal and orthorhombic phases coexist.[16] Some of these publications have shown the relaxor-like character of the phase-transition of these materials.[17] Besides, PCT ceramics with Ca^{2+} contents close to 50 at% have a ferro-paraelectric transition close to room temperature with high ε' values.

Works on preparation and properties of PCT thin films have always made emphasis on compositions with low Ca^{2+} contents and on their ferroelectric properties and their pyroelectric and piezoelectric responses[18-21]. Nobody has previously considered that PCT thin films with Ca^{2+} contents of ~50 at% should have a high charge storage and

varactor characteristics that would be useful in DRAM and tunable components, respectively.

To the authors' knowledge, PCT thin films with Ca^{2+} contents of 50 at% have not been reported. The reason for this must be related with the problems that the techniques used for the preparation of PCT thin films present when large Ca^{2+} contents must be added. Physical deposition methods usually lead to films with a bad-adjusted stoichiometry, due to the different vapour pressure of the elements and the preferential sputtering of Pb. Compatibility among starting reagents in a stable solution is the main problem of CSD methods. Besides, in the PCT system the calcium precursor is an additional problem, since calcium compounds are not soluble in the solvents usually used in CSD (alcohols or carboxylic acids). Calcium has been added to PCT solutions as a metal[22-23], an acetate[20,24-26], an acetylacetonate[27], a carbonate[19,28-29] or a nitrate[25,30-32]. But, all these CSD methods have clearly shown the difficulty of preparing precipitate-free precursor solutions with Ca^{2+} contents over 25 at%. By CSD, only some of the authors of this work[21], F.M.Pontes *et.al.*[19] and H.Li *et.al.* [20] have prepared PCT films with a maximum Ca^{2+} content of 40 at%. Pontes *et.al.* used a precursor polymeric method based on the Pechini route[28] that leads to ferroelectric perovskite PCT films, whereas Li *et.al.* used a sol-gel method that produced films with a non-ferroelectric pyrochlore structure. Therefore, fabrication by CSD of ferroelectric PCT films with large Ca^{2+} contents have difficulties derived from the low stability of the solutions and the formation of non-ferroelectric phases during the crystallisation of the perovskite film. The authors of this work have recently shown preliminary results on preparation by CSD and properties of PCT thin films with Ca^{2+} contents close to 50 at%[33-34], using a diol-based sol-gel route[25,35-37], that overcomes the problems related with the introduction of large amounts of Ca^{2+} in this composition.

In this paper, we introduce the preparation of calcium lead titanate thin films with Ca^{2+} contents of ~50 at%, and show that their properties make them promising alternative dielectrics for applications in high frequency tunable components and dynamic random access memories (DRAM). A detailed description of the chemical processes developed in our laboratory for the introduction of large amounts of Ca^{2+} in these films is shown.

2. Experimental

2.1. Solutions

Three different solution processes, all based on the diol-sol-gel route[25,35-37], were tested here for the synthesis of calcium-modified lead titanate (PCT) precursor solutions with nominal composition of $Pb_{0.50}Ca_{0.50}TiO_3$. Differences among the three processes reside in the way that calcium is incorporated to the chemical system: 1) as a water solution of calcium acetate hydrate $Ca(OCOCH_3)_2.xH_2O$ (Aldrich, 99,99%) [25,37] (route a), 2) as a diol-water solution of calcium acetate hydrate (route b) or 3) as a diol-water solution of calcium acetylacetonate hydrate $Ca(CH_3COCHCOCH_3)_2.xH_2O$ (Aldrich) [27] (route c). Lead (II) acetate trihydrate $Pb(OCOCH_3)_2.3H_2O$ (Aldrich, 99%) and titanium di-isopropoxide bis(acetylacetonate) $Ti(OC_3H_7)_2(CH_3COCHCOCH_3)_2$ (Aldrich, 75 wt% solution in 2-propanol) were used as reagents of lead (II) and titanium (IV), respectively. 1,3-propanediol, $OH(CH_2)_3OH$, (Aldrich, 98%) and deionised water, H_2O, were used as solvents. The molar ratio of Pb:Ca:Ti was kept at 0.50:0.50:1.00. A 10 mol% excess of PbO was used[38], as well as a molar ratio of Ti(IV):1,3-propanediol of 1:5[39]. Figure 1 shows the schematic diagrams of the three routes.

In the route a (Fig.1a), lead acetate trihydrate and 1,3-propanediol were refluxed at ~428 K in air for 1 hour. Titanium di-isopropoxide bis(acetylacetonate) was added to this mixture and reflux in air at ~383 K was maintained for 8 hours. After reflux, byproducts

of reaction were distilled off, obtaining a clear and stable Pb(II)-Ti(IV) sol. Calcium acetate hydrate dissolved in water, H_2O, (molar ratio of water to 1,3-propanediol of 7 to 1) was incorporated to this sol at room temperature. After stirring, a precipitate-free stock Ca(II)-Pb(II)-Ti(IV) solution, containing the equivalent of ~0.90 mol of $Pb_{0.5}Ca_{0.5}TiO_3$ per litre and a density of ~1.30 kg/L, was obtained. This solution and gels and films derived from it are denoted PCT-A.

In the route b (Fig. 1b), calcium acetate hydrate and lead (II) acetate trihydrate were refluxed at ~378 K in a mixture of 1,3-propanediol and water (molar ratio of water to 1,3-propanediol of 7 to 1) for 1 hour in air. After reflux, titanium di-isopropoxide bis(acetylacetonate) was added to the former mixture, continuing reflux in air at ~363 K for 8 hours. After completing reflux, distillation of byproducts was carried out. A precipitate-free stock solution with the equivalent of ~0.90 mol of PCT per litre and a density of ~1.30 kg/L was obtained. This solution and gels and films derived from it are denoted PCT-B.

The chemical process followed in the route c (Fig. 1b) was the same than that of the route b, with the only difference that calcium acetylacetonate was used as reagent. Molar ratios of water to 1,3-propanediol up to 10 to 1 were used. In this case, it was not possible to get precipitate-free PCT solutions. The testing of different calcium contents revealed that, by this route, only transparent solutions with Ca^{2+}<25 at% could be obtained.

The precursor solutions obtained through the routes a and b had a golden colour and were free of precipitate for months. Inductively coupled plasma (ICP) mass spectrometry was used to confirm the concentration of the different elements in the stock solutions, which was in agreement with the concentration obtained by conventional gravimetric methods.

Viscosity measurements were carried out at 298 K in the former solutions using shear rates between 375 s^{-1} and 1875 s^{-1}. Particle size distributions in the solutions were obtained by means of Dynamic Light Scattering (DLS).

Samples of the stock solutions derived from routes a and b, and their distilled liquids were analyzed by Fourier transform infrared spectroscopy (FT-IR) (Nicolet FT-IR 20SXC). Aliquots of these solutions were also dried at 373 K for 12 hours and subjected to thermogravimetric and differential thermal analysis (TGA/DTA) (Seiko 320U) between 373 K and 1273 K, in an air-flux and with a heating rate of ~10 K/min.

2.2. Thin films

Diluted solutions with an equivalent of 0.3 mol of PCT per litre were prepared by adding water as solvent. Diluted solutions were deposited by spin-coating at 2000 rpm for 45 s onto $Pt/TiO_2/SiO_2/(100)Si$ substrates. Wet films were dried on a hot plate at 623 K for 60 s. Crystallisation of the deposited films was carried out by rapid thermal processing (RTP) (JIPELEC JetStar 100T equipment) in air at 923 K for 50 s, with a heating rate of ~30 K/s. Solution layers were successively deposited, dried and crystallised to obtain films with the desired thickness. After the deposition of the last layer, the films were treated by RTP at 923 K, but for a time of 1 hour.

Crystalline phases of the films were analysed by x-ray diffraction (XRD) in Bragg-Brentano geometry. A powder Siemens D500 diffractometer with a Cu anode was used.

Films surfaces were studied by Scanning Probe Microscopy (SPM). Surface roughness and grain size were calculated from the topographic images obtained with a Nanotec SPM, working in tapping mode with a cantilever of spring constant of 0.73 N/m and resonance frequency of 71 kHz.

The average thickness of the crystalline films was measured by profilometry (Taylor-Hobson Talysurf 50 profilometer). Thickness measurements were also carried out on cross-section samples by scanning electron microscopy (SEM) (Philips XL 30).

Compositional profile and film-substrate interface were analysed by Rutherford backscattering spectrometry (RBS). A 3 MV Tandem accelerator was used with a 2 MeV $^4He^{2+}$ beam and a silicon surface barrier detector set at 165º. The RBS experimental data were analysed with the RUMP simulation code[40]. The density of platinum used for the calculation of thickness of the Pt bottom electrode was the theoretical one of 21.45×10^{-3} g/cm^3. Average film composition was calculated by RBS with an estimated error of ~10%. This is not low enough to get an accurate composition of the crystalline film. However, information provided by RBS about film profile (mainly, about formation of top or bottom interfaces) is very valuable, since this profile is directly related with the performance of the film in devices (DRAM, varactors, ….).

Top Pt electrodes of 5×10^{-8} m^2 were sputtered (BAL-TEC SCD 050 sputter coater) on the films surfaces, using a shadow mask. These capacitors were subjected to a treatment in oxygen by RTP at 773 K, previous to the dielectric characterisation. Variation of complex dielectric permittivity, ε^*, was measured as a function of temperature and frequency (LCR-meter HP 4284A), using a home made nitrogen cryostat. Leakage current densities were measured at room temperature for different positive and negative voltages, under the step relaxation technique (electrometer Keithley 6512 and function generator HP3325B). tan δ and variation of capacitance with dc bias voltage (C-V curves) were measured at several temperatures, with a frequency of 10^4 Hz, within the dc bias range of ±39 V and a dc voltage amplitude of 0.05V (impedance analyser HP 4194A).

3. Results

Fig.2 shows the IR spectra of the distilled liquids from the reaction solutions and the PCT precursor solutions, obtained by the routes a and b. IR spectra of the distilled liquids (Fig.2a) indicate that, in both routes, byproducts of the reactions are water (H_2O), 2-propanol ($(CH_3)_2CHOH$), acetic acid (CH_3COOH) and isopropylacetate ($(CH_3)_2CHCOOCH_3$).[37,38] Water is observed through the broad band at ~3400 cm^{-1} corresponding to the ν(O-H) stretching vibrations and the δ(O-H-O) bending mode detected at ~1622 cm^{-1}. The mode ν(O-H)~3400 cm^{-1} is also characteristic of alcohols ($(CH_3)_2CHOH$). 2-propanol is also detected by the ν(C-H) and ν(C-O(H)) vibrations observed between ~2975 and ~2926 cm^{-1}, and ~945 cm^{-1}, respectively, and the δ($-CH_3$) bending mode at 1375 cm^{-1}. The band at ~1710 cm^{-1} can be assigned to the ν(C=O) stretching vibrations of acetic acid. Besides, during the syntheses reactions, isopropylacetate can be formed between the acetate ligands of the calcium and/or lead reagents, and the isopropyl ligand of the titanium reagent. The ν(C=O) stretching vibration that appears between ~1740 and ~1730 cm^{-1} can be assigned to this ester (see inset of Fig.2a).

The IR spectra of the PCT precursor solutions (Fig.2b) indicates that titanium remains bonded in the synthesised solutions to the acetylacetonate groups, as shown by the combined bands ν(C-C)+ν(C-O)~1580 cm^{-1} and ν(C-O)+ν(C-C)~1535 cm^{-1}, and the mode δ($-CH_3$)+ν(C-C)~1425 cm^{-1}.[37] However, the ν(C-H) vibrations between ~2935 cm^{-1} and ~2885 cm^{-1}, and ν(C-O(H))~930 cm^{-1} corresponding to the isopropyl ligand, are here clearly lower than those of the 2-propanol detected in the IR spectra of the distilled liquids. This indicates the rupture of the bonds between titanium and isopropyl groups of the $Ti(OC_3H_7)_2(CH_3COCHCOCH_3)_2$ reagent. Isopropyl ligands are distilled off from the solution as 2-propanol. The appearance in the IR spectra of the solutions, of

the ν(C=O) stretching vibrations at ~1740-1730 cm^{-1} (see inset of Fig.2b) and ~1710 cm^{-1} corresponding to the isopropylacetate ester and the acetic acid, respectively, again indicates the rupture of the bonds between lead or calcium, and the acetate ligands of the $Pb(OCOCH_3)_2.3H_2O$ and $Ca(OCOCH_3)_2.xH_2O$, and the formation of the isopropylacetate ester. Here, these bands show that neither free acetic acid nor isopropylacetate are totally distilled from the solutions. Modes corresponding to the 1,3-propanediol and the water solvents [ν(O-H)~3400 cm^{-1} of water and diol, ν(C-O(H))~1060 cm^{-1} of 1,3-propanediol] are also observed in the spectra of Fig.2b. Metal – oxygen vibrations could be assigned to the weak bands observed below 700 cm^{-1}.

Figure 3 shows the particle size distributions obtained by means of DSL in the stock solutions (Fig.3a) and their viscosity as a function of shear rate (Fig.3b), measured at room temperature. Note that rheological properties of the two solutions are different. The solution derived from the route a is formed by a broad and asymmetrical particle size distribution with a mean size of ~35 nm, whereas the other solution has a narrow and symmetrical particle size distribution with a mean value of ~15 nm. As a consequence, the two solutions have different viscosity values. The solution with small particles (route b) has a lower viscosity, η~14 mPa.s, than that of η~40 mPa.s measured in the other solution with larger and heterogeneous particles (route a). Viscosity is independent of the shear rate for both solutions, indicating that they are Nwetonian fluids. Besides, the heterogeneity in particle size of the solution derived from the route a is not due to particle aggregation, since this would produce a decrease in viscosity as the shear rate increases.[41]

Figure 4 shows the thermal analysis of the gels derived from the stock solutions. Three different thermal decomposition intervals can be distinguished in the TGA/DTA curves. Below 473 K, evaporation of water and alcohol contained in the pores of the gels takes

place, which is associated to a weak endothermic peak in the DTA curves at ~330 K and a small weight loss (~7.51 wt%). The largest weight loss is measured for both gels in the temperature interval between 473 and 723 K (~22.36 wt% for the PCT50-A gel and ~22.50 wt% for the PCT50-B gel). Here, elimination of organic compounds occurs in the two chemical systems. It seems that, in the PCT-A gel, this elimination is produced through a two-step process that is associated to two clearly differentiated exothermic peaks recorded at 563 K and 648 K. However, in the PCT-B gel, a much higher single exothermic peak at 613 K is recorded, in which a shoulder at 573 K can be distinguished. Over 723 K, small weight losses are detected in both systems. They are associated to the elimination of organic residuals and are slightly larger in the PCT-A gel (~6.28 wt%) than in the PCT-B gel (~5.13 wt%).

Figure 5 shows the XRD patterns and the SPM topographic images of PCT-A and PCT-B crystalline films with thickness over a micron. Both films have a pseudocubic structure. Noticeable second phases are not detected in the x-ray patterns. The SPM images show homogeneous microstructures without morphological differentiated second phases. Both films have an average grain size of ~50 nm, as measured from the SPM images of their surfaces.

The RBS experimental spectra of the former films and their corresponding simulations are depicted in Fig.6. A good fit between the experimental and the simulated curves is obtained. Films heterostructures deduced from these analyses and cross-section SEM images of the films are also shown in this figure. The RBS data indicate that the films processed by the route a (PCT-A film) have a larger content of lead than the films processed by the route b (PCT-B film). A simulated curve considering an elemental composition of 0.45Pb+0.50Ca+1.00Ti+3.00O (error ~10%) fits well with the experimental data for the film PCT-B. This film has a homogeneous compositional

profile. However, the film PCT-A has a heterogeneous compositional profile where an interface between the PCT layer and the Pt bottom electrode is detected. The thickness of this interface is about 13% of the total film thickness and has an elemental composition of 0.50Pb+0.50Ca+1.00Ti+3.00O+0.10Pt (error ~10%). Total thickness of the films has been obtained by calculating the average of the film thickness calculated from the SEM images and those measured by profilometry. An average thickness of ~1350 nm was obtained for both films (PCT-A and PCT-B films). The thickness of the Pt bottom electrode has been calculated from the RBS data (Fig.6).

Variation of dielectric constant (ε') with temperature at different frequencies is shown in Fig.7, comparatively for the films PCT-A and PCT-B analysed by RBS. Note that the film PCT-B has larger values of ε' than the film PCT-A. The former has a ε' of ~562 at room temperature, whereas the latter has a ε' of ~392. Both films have a diffuse ferro-paraelectric transition with a relaxor-like character. As the PCT-B film looks more promising for applications due to its higher ε' values, we study its leakage currents (inset of Fig.7), which are below 10^{-8} A.cm^{-2} for the range of applied electric fields used in the measurements.

Capacitance vs voltage (C-V) curves of the PCT-B film are shown in Fig.8 for two different temperatures: 253 K (Fig.8a), below the ferro-paraelectric transition temperature, and 373 K (Fig.8b), above the ferro-paraelectric transition temperature. Fig.8c shows the temperature dependence of tunability and figure of merit which were calculated using eq.(1) and eq.(2), respectively. Variation with temperature of tan δ, is shown in the inset of Fig.8c.

4. Discussion

Different calcium reagents have been tested in the literature for the synthesis of PCT precursor solutions, only for Ca^{2+} contents below 40 at%. But, the difficulties found in getting a transparent solution with calcium acetylacetonate[27] or metallic calcium precursors[22-23], and the complex decomposition processes of PCT gels derived from calcium carbonate[19,28-29] or calcium nitrate[25,30-32], make difficult to obtain precipitate-free PCT solutions with high Ca^{2+} contents. The routes developed by the authors here point to the use of calcium acetate as one of the more appropriate reagents for the synthesis of these solutions with large amounts of calcium. Only routes a and b of Fig.1 lead to precipitate-free solutions. Route c is unable to produce optimum solutions and had to be withdrawn. But, differences are found if the calcium acetate is simply mixed with the synthesised Pb(II)-Ti(IV) sol (route a, Fig.1a) or if it is reacted with Pb(II) and Ti(IV) to form a Ca(II)-Pb(II)-Ti(IV) sol (route b, Fig.1b). In the latter, the three cations participate in the sol network giving rise a more homogenenous precursor solution with a narrow particle size distribution and a mean particle size of ~15 nm (Fig.3a). On the contrary, the solution derived from the route a (PCT-A) is not a real sol. It is a mixture of an aqueous solution of calcium acetate and a Pb(II)-Ti(IV) sol. Water from the aqueous solution produces non-controlled hydrolysis reactions in the mixture. This leads to the formation of heterogeneous particles with different sizes and with a mean size of ~35 nm, larger than that of the Ca(II)-Pb(II)-Ti(IV) sol synthesised by the route b (solution PCT-B). As a consequence, the solution PCT-A has also a larger viscosity (Fig.3b). IR results of Fig.2 show that during the synthesis of the Ca(II)-Pb(II)-Ti(IV) sol, the acetic acid and the isopropylacetate ester distilled off (Fig.2) are partially formed with the acetate groups coming from the rupture of the calcium-acetate bonds, whereas in the PCT-A solution this calcium acetate remains dissolved in the solution.

This contributes to the heterogeneity of the solution PCT-A that is reflected in a more complicate thermal decomposition than that of the solution PCT-B (Fig.4). The DTA curve of the former (Fig.4a) shows a two-steps decomposition process whereas the DTA of the latter (Fig.4b) shows a simpler decomposition path. Besides, weight losses of the PCT-A gel during its thermal decomposition are slightly larger than those of the PCT-B gel. Moreover, these larger weight losses are concentrated at temperatures >723 K (6.28% for the PCT-A gel and 5.13% for the PCT-B gel), where decomposition of calcium carbonate, $CaCO_3$, is produced[42]. This is an intermediate compound of the calcium acetate pyrolysis[43] and its presence here, up to high temperatures, indicates that Ca(II) is as calcium acetate in the solution PCT-A and that has not totally been incorporated to the gel network.

The SPM images and the x-ray diffraction patterns of Fig.5 seem to indicate that both precursor solutions produce films with similar microstructures and structures. Morphological or structural differentiated second phases are not detected. Both type of films have a pseudocubic structure with a (100) preferred orientation. Relatively larger intensity of the 100 peak is obtained in the film PCT-A than in the film PCT-B.

A detailed RBS study of the film heterostructures, clearly shows differences from one film to another, most probably due to the differences in the solutions homogeneity above discussed. Appreciable differences in the thickness of the films are not detected, in spite of the different viscosities of the solutions. However, note that the film PCT-A, derived from the route a, has a heterogeneous profile: a top surface with less lead than the bulk film and a bottom interface formed between the film and the Pt electrode. However, the film derived from the homogeneous sol (route b) has a homogeneous compositional profile with a slightly lower content of lead than the former film, and with an average elemental composition close to the stoichiometric one (see Fig.6).

Assuming that a single perovskite phase is formed, we could represent the composition of this film deduced from RBS as close to $Pb_{0.45\pm0.05}Ca_{0.50\pm0.05}Ti_{1.00\pm0.10}O_{3.00\pm0.30}$, where the Ca^{2+} content maintains ~50 at%. Homogeneous compositional profiles have also been experimentally observed in our laboratory for other PCT films with lower calcium contents, but prepared following the same synthetic route b of the present work. This establishes a relation between solution homogeneity and film homogeneity. The bottom interface developed in the film PCT-A and not in the film PCT-B, could lead to the slightly different textures detected in both films by x-ray diffraction (Fig.5). But also, this interface is related with the different dielectric properties measured in the films. The contribution of the bottom interface in the film PCT-A makes that ε' values are much lower for this film than for the film PCT-B. The ε' values of the film PCT-B are over 500. These values, as expected, are lower than those of bulk ceramics (800-1500, at room temperature)[44], but are larger than those reported for PCT films with calcium contents of ~40 at% (~400)[19,29] and close to those measured at room temperature in BST films with similar thickness, which rarely exceed 600 in polycrystalline films[45] . The ε' values of the PCT-B film together with the leakages measured on it, which are lower than 10^{-8} A.cm^{-2} (inset of Fig.7), indicates the suitability of this type of films for their use in DRAM. It is well known that the storage of charge in DRAM devices improves with the decrease of film thickness. Thus, films with thickness lower than 100 nm are required, although they always have lower ε' values than those of thicker films. Therefore, a compromise has to be taken between thickness and performance of the film in a DRAM. Here, for this particular application, thinner films with thickness below 100 nm were also prepared following the route b. Leakages of ~10^{-8} A.cm^{-2} and a ε' value at room temperature of ~225 were measured in a ~80 nm thick film. These results confirm

again the utility of these PCT films in DRAM devices where a high charge storage is required.

The larger ε' values obtained in the films PCT-B indicates that these films derived from the route b are the more appropriate also for tunable applications. Therefore, the dependence of the capacitance with the voltage has been only studied in the film PCT-B (Figs.8a and 8b). Losses measured in this film (inset of Fig.8c) maintain below 0.02. They are similar to those measured in polycrystalline BST films. Values of tunability shown in Fig.8c change not more than 10% with temperature. Figure of merit is close to 40% and increases with the temperature. This is due to the relaxor-like character of these films that produce a decrease of losses with the increase of temperature (see inset of Fig.8c). These tunability and figure of merit values are comparable to those reported for other alternative materials[1,2], thus showing the potential use of these films in tunable components.

5. Conclusions

Calcium lead titanate, (Pb,Ca)TiO_3, precipitate-free solutions containing calcium contents of 50 at% have been synthesised by a diol-based sol-gel process, using calcium acetate, $Ca(OCOCH_3)_2.xH_2O$, as reagent, which has been proved to be the most appropriate form to introduce large amounts of calcium in this system. One of the synthesis routes proposed in this work, based on the formation of a Pb(II)-Ti(IV)-Ca(II) sol provides a homogeneous solution in which thermal decomposition is simpler than that of a solution formed by the mixture of a Pb(II)-Ti(IV) sol and a calcium acetate water solution. This mixture provides a solution formed by heterogeneous particles with a mean size and a viscosity larger than those of the Pb(II)-Ti(IV)-Ca(II) sol. As a result,

films derived from the Pb(II)-Ti(IV)-Ca(II) sol have a homogeneous compositional profile without bottom interfaces, like the ones derived from the other route.

The non-existence of bottom interfaces in the films derived from the Pb(II)-Ti(IV)-Ca(II) sol together with the large Ca^{2+} content of ~50 at%, make that these films have high dielectric constants and a diffuse ferro-paraelectric transition close to room temperature. This behaviour and the low leakage currents (below 10^{-8} $A.cm^{-2}$) make these films promising for DRAM applications. Besides, the low dielectric losses (below 0.02) and the relatively high dielectric constants measured in the films provide tunabilities and figures of merit similar to those reported for other more traditional materials used in tunable components.

Acknowledgments. This work has been supported by the Spanish projects MAT2001-1564 and CAM 07N/0084/2002. The authors would like to thank Dr. R. Sirera of Univ. of Navarra (Spain), for the measurements of particle size in solution by DLS. R.Jiménez, J.Ricote and J.García-López acknowledge the financial support of the Ramón y Cajal Spanish MCyT program.

References

[1] A.I.Kingon, J.P.Maria and S.K.Streiffer. *Nature*, **406**, 1032-1038 (2000).

[2] D.Dimos and C.H.Mueller. *Ann.Rev.Mater.Sci.*, **28**, 397-419 (1998).

[3] S.B.Majumder, M.Jain, A.Martinez, R.S.Katiyar, F.W.Van Keuls and F.A.Miranda. J.Appl.Phys., **90(2)**, 896-903 (2001).

[4] J.G.Cheng, X.J.Meng, J.Tang, S.L.Guo and J.H.Chu. Appl.Phys.A., **70**, 411-414 (2000).

[5] J.G.Cheng, T.Tang, A.J.Zhang, X.J.Meng and J.H.Chu. Appl.Phys.A., **71**, 667-670 (2000).

[6] T.J.Zhang and H.Ni. J.Mater.Sci., **37**, 4155-4158 (2002).

[7] J.Hao, W.Si and X.X.Xi. *Appl.Phys.Lett*., **76(21)**, 3100-3102 (2000).

[8] V.V.Lemanov, A.V.Sotnikov, E.P.Smirnova and M.Weihnacht. *Appl.Phys.Lett*., **81(5)**, 886-888 (2002).

[9] J.Mendiola, B.Jiménez, C.Alemany, L.Pardo and L.del Olmo. *Ferroelectrics*, **94**, 183-188 (1989).

[10] Y.Ito, h.Takeuchi, S.J.Jyomura, K.Nagatsuma and S.Ashida. *Appl.Phys.Lett*, **35**, 595-597 (1979).

[11] T.Yamamoto, M.Saho, K.Okazaki and E.Goo. *Jpn.J.Appl.Phys*., **26**, 57-60 (1987).

[12] D.Damjanovic, T.G.Gururaja and L.E.Cross. *Am.Ceram.Soc.Bull*., **66**, 699-703 (1987).

[13] K.M.Rittenmyer and R.Y.Ting. *Ferroelectrics*., **110**, 171-182 (1990).

[14] B.Jiménez and R.Jiménez. *Phys.Rev.B*, **66**, 014104-1-014104-7 (2002).

[15] I.W.Su, C.C.Chou and D.S.Tsai. *Integrated Ferroelectrics*, **48**, 69-78 (2002).

[16] A.Chandra and D.Pandey. *J.Mater.Res*., **18(2)**, 407-414 (2003).

[17] R.Ranjan, N.Singh, D.Pandey, V.Siruguri, P.S.R.Krishna, S.K.Paranjpe and A.Banerjee. *Appl.Phys.Lett*., **70(24)**, 3221-3223 (1997).

[18] E.Yamaka, H.Watanabe, H.Kimura, H.Kanaya and H.Ohkuma. *J.Vac.Sci.Technol.A*, **6(5)**, 2921-2928 (1988).

[19] F.M.Pontes, D.S.L.Pontes, E.R.Leite, E.Longo, E.M.S.Santos, S.Mergulhao, A.Chiquito, P.S.Pizani, F.Lanciotti Jr, T.M.Boschi and J.A.Varela. *J.Appl.Phys*., **91(10)**, 6650-6655 (2002).

[20] H.Li, X.Tang, Q.Li, Y.Liu, Z.Tang, Y.Zhang and D.Mo. *Solid State Communications*, **114**, 347-350 (2000).

[21] A.L.Kholkin and M.L.Calzada. *J.Phys.IV France*, **8**, 195-198 (1998).

[22] A.Tsuzuki, H.Murakami, K.Kani, K.Watari and Y.Torii. *J.Mater.Sci.Lett*., **10**, 125-128 (1991).

[23] Y.Torii, A.Tsuzuki, H.Murakami. *J.Mater.Sci.Lett*., **13**, 1364-1366 (1994).

[24] R.Sirera, M.L.Calzada, F.Carmona and B.Jiménez. *J.Mater.Sci.Lett*., **13**, 1804-1805 (1994).

[25] R.Sirera and M.L.Calzada. *Mater.Res.Bull*., **30(1)**, 11-18 (1995).

[26] H.Shen, J.Chen and G.Chen. *J.Non-Cryst.Solids* , **220**, 231-234 (1997).

[27] C.M.Wang, Y.T.Huang, Y.C.Chen, M.S.Lee and M.C.Kao. *Jpn.J.Appl.Phys*., **39**, 3579-3583 (2000).

[28] D.S.L.Pontes, E.R.Leite, F.M.Pontes, E.Longo and J.A.Varela. *J.Eur.Ceram.Soc*., **21**, 1107-1114 (2001).

[29] F.M.Pontes, D.S.L.Pontes, E.R.Leite, E.Longo, A.J.Chiquito, M.A.C.Machado, P.S.Pizani and J.A.Varela. *Appl.Phys.A*., **78**, 349-354 (2004).

[30] S.Chewasatn and S.J.Milne. *J.Mater.Sci.*, **32(3)**, 575-582 (1997).

[31] D.Bao, X.Wu, L.Zhang and X.Yao. *Thin Solid Film*s, **350**, 30-37 (1999).

[32] D.Bao, L.Zhang and X.Yao. *Appl.Phys.Lett*., **76(8)**, 1063-1065 (2000).

[33] M.L.Calzada, I.Bretos, R.Jiménez, J.Ricote and J.Mendiola. *Thin Solid Films*, **450**, 211-215 (2004).

[34] J.Mendiola, R.Jiménez, P.Ramos, C.Alemany, M.L.Calzada and E.Maurer. *Proceedings of First International Meeting of Applied Physics*. Oct.2003. Badajoz-Spain (in press).

[35] N.J.Phillips and S.J.Milne. *J.Mater.Chem*., **1(5)**, 893-894 (1991).

[36] N.J.Phillips, M.L.Calzada and S.J.Milne. *J.Non-Cryst.Solids*., **147-148**, 285-290 (1992).

[37] R.Sirera. *PhD Thesis*. Univ. Autónoma de Madrid, 1997.

[38] C.C.Hsueh and M.L.Mecartney. *J.Mater.Res*., **6(10)**, 2208-2217 (1991).

[39] M.L.Calzada and R.Sirera. *J.Mater.Sci. Mater.Elect*., **7**, 39-45 (1996).

[40] L.R.Doolittle. *Nucl.Instr.and Meth*. 1985, **15(1-6)**, 227-231 (1986).

[41] A.G.Fredrickson. *Principles and applications of rheology*. Ed.by Prentice-Hall Inc., Englewood Cliffs, NJ (1964).

[42] M.L.Calzada, B.Malic, R.Sirera and M.Kosec. *J.Sol-Gel Sci.Techn*., **23**, 221-230 (2002).

[43] B.Malic, M.Kosec, K.Smolej and S.Stavber. *J.Eur.Ceram.Soc*., **19**, 1345-1348 (1999).

[44] Y.Yamashita, K.Yokoyama, H.Honda and T.Takahashi. *Jpn.J.Appl.Phys*., **20**, 183-187 (1981).

[45] J.G.Cheng, X.J.Meng, B.Li, J.Tang, S.L.Guo, J.H.Chu, M.Wang, H.Wang and Z.Wang. *Appl.Phys.Letts*., **75(14)**, 2132-2134 (1999).

Figure captions

Figure 1. Different processing routes of the PCT solutions.

Figure 2. IR spectra of a) the distilled liquids and b) the precursor solutions. Insets correspond to the wavenumber interval where the ν(C=O) stretching vibrations of acetic acid (~1710 cm^{-1}) and isopropylacetate ester (~1740-1730 cm^{-1}) are observed.

Figure 3. a) Particle size distributions obtained by DLS in the solutions derived from the route a and route b. b) Viscosity of the solutions derived from the routes a and b, as a function of shear rate.

Figure 4. TGA/DTA curves of a) gels derived from solutions of route a and b) gels derived from solutions of route b.

Figure 5. SPM images and XRD patters of a) the films PCT-A and b) the films PCT-B.

Figure 6. RBS spectra and heterostructures deduced from RBS data for the films PCT-A and PCT-B. SEM cross-section images of the films PCT-A and PCT-B are included in the figure.

Figure 7. Variation of dielectric constant, ε', with temperature and frequency for the films derived from the route a (PCT-A) and from the route b (PCT-B). Inset shows the leakage current behaviour of the film PCT-B, measured at room temperature.

Figure 8. Capacitance-Voltage (C-V) curves for the film PCT-B measured at a) 253 K and b) 373 K. c) Tunability and figure of merit of the film PCT-B measured at different temperatures and a frequency of 10^3 Hz. Inset of the Fig.7c shows the losses (tan δ) of the film PCT-B at different temperatures.

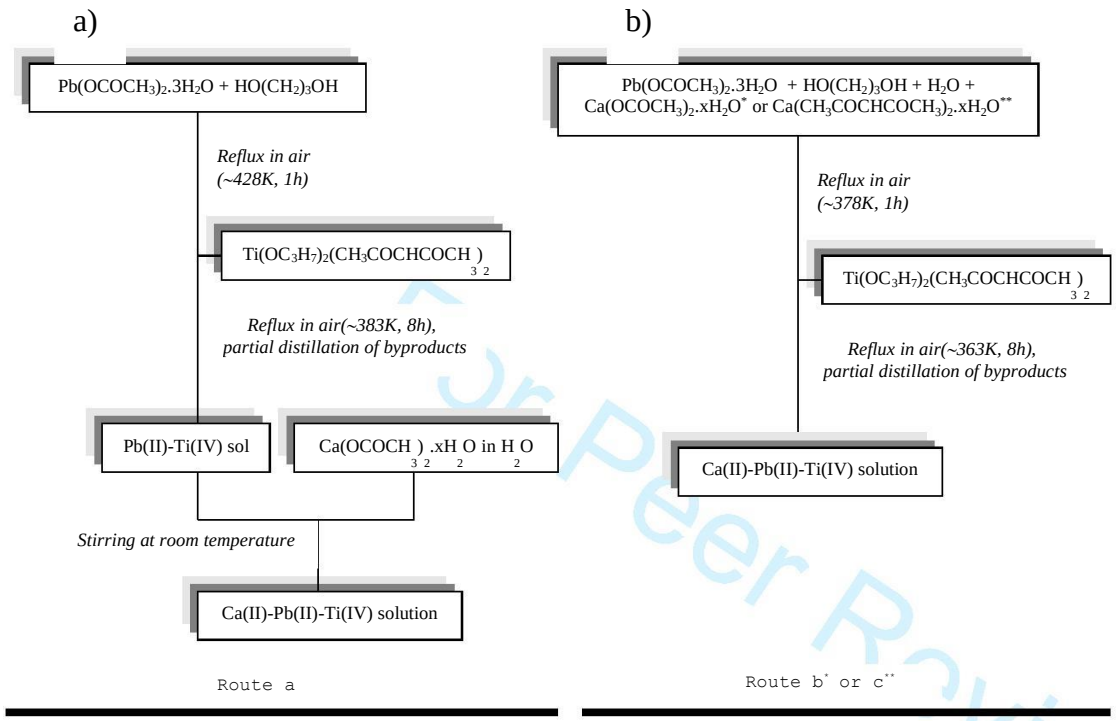

Figure 1

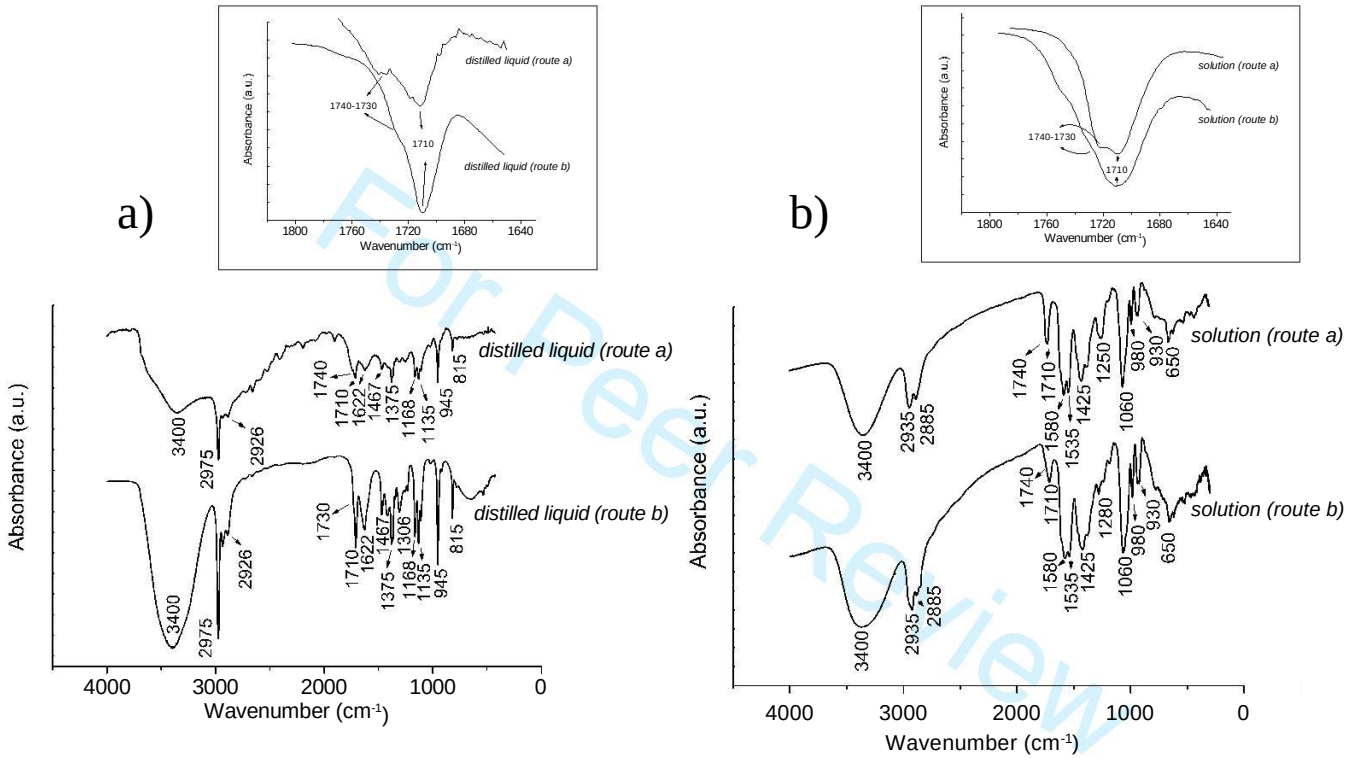

Figure 2

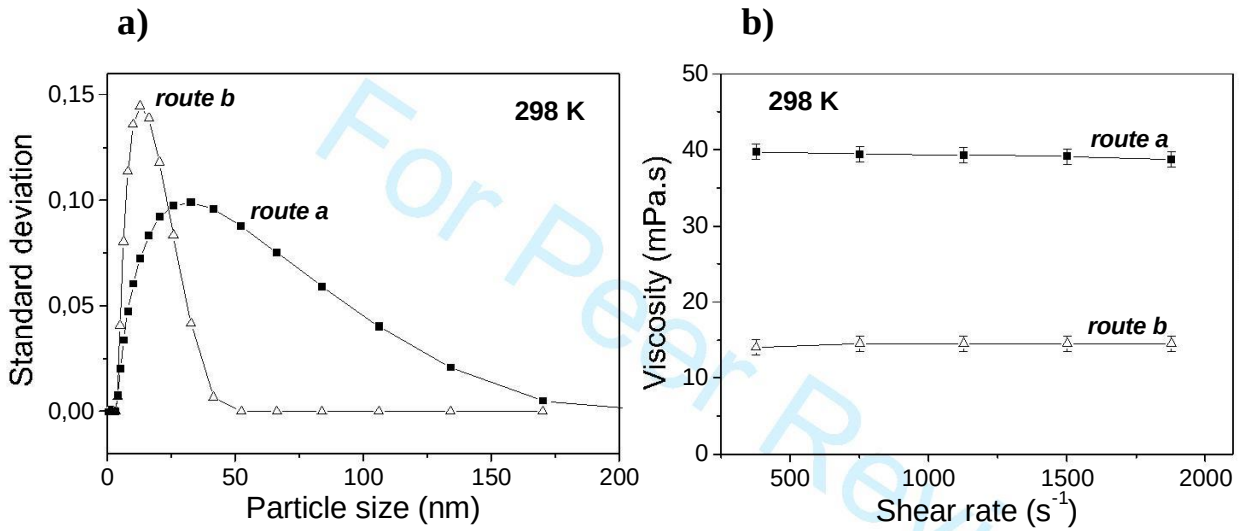

Figure 3

a)

Temperature interval (K)	weight loss (%)
<473	7.51
473-723	22.36
>723	6.28
TOTAL	36.15

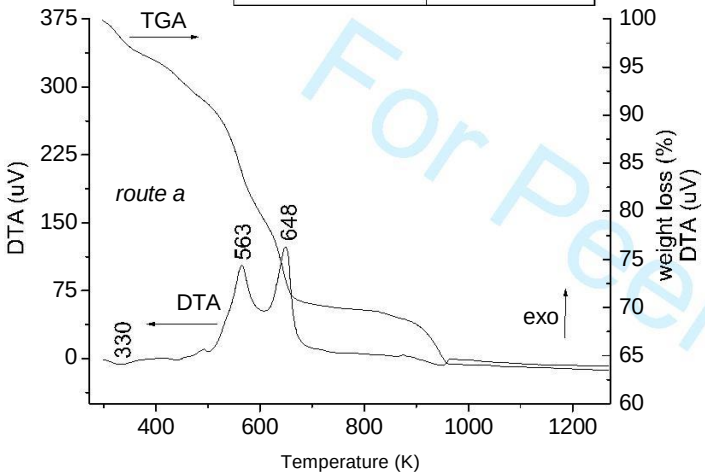

b)

Temperature interval (K)	weight loss (%)
<473	7.51
473-723	22.50
>723	5.13
TOTAL	35.14

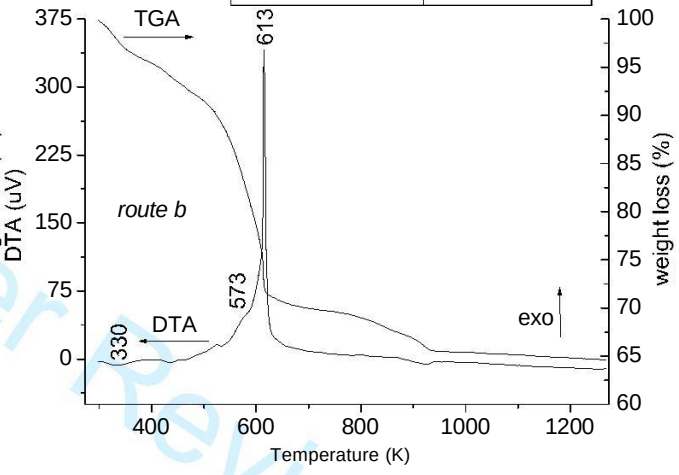

Figure 4

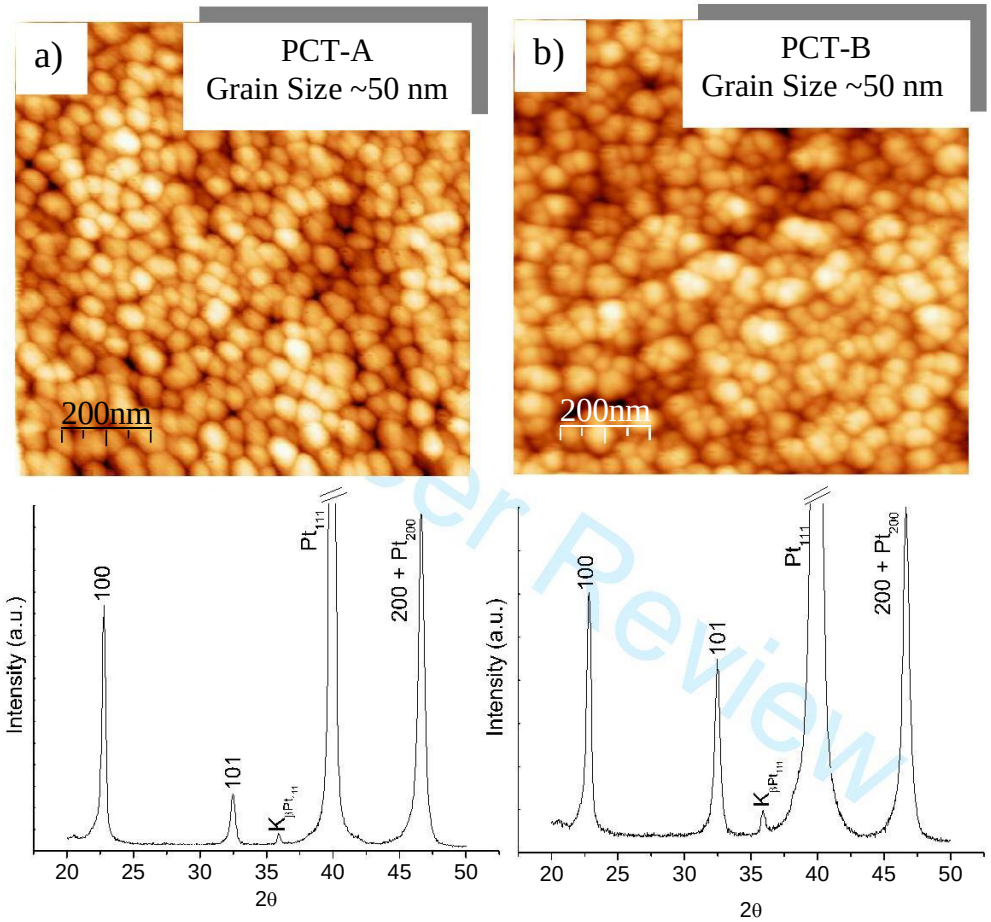

Figure 5

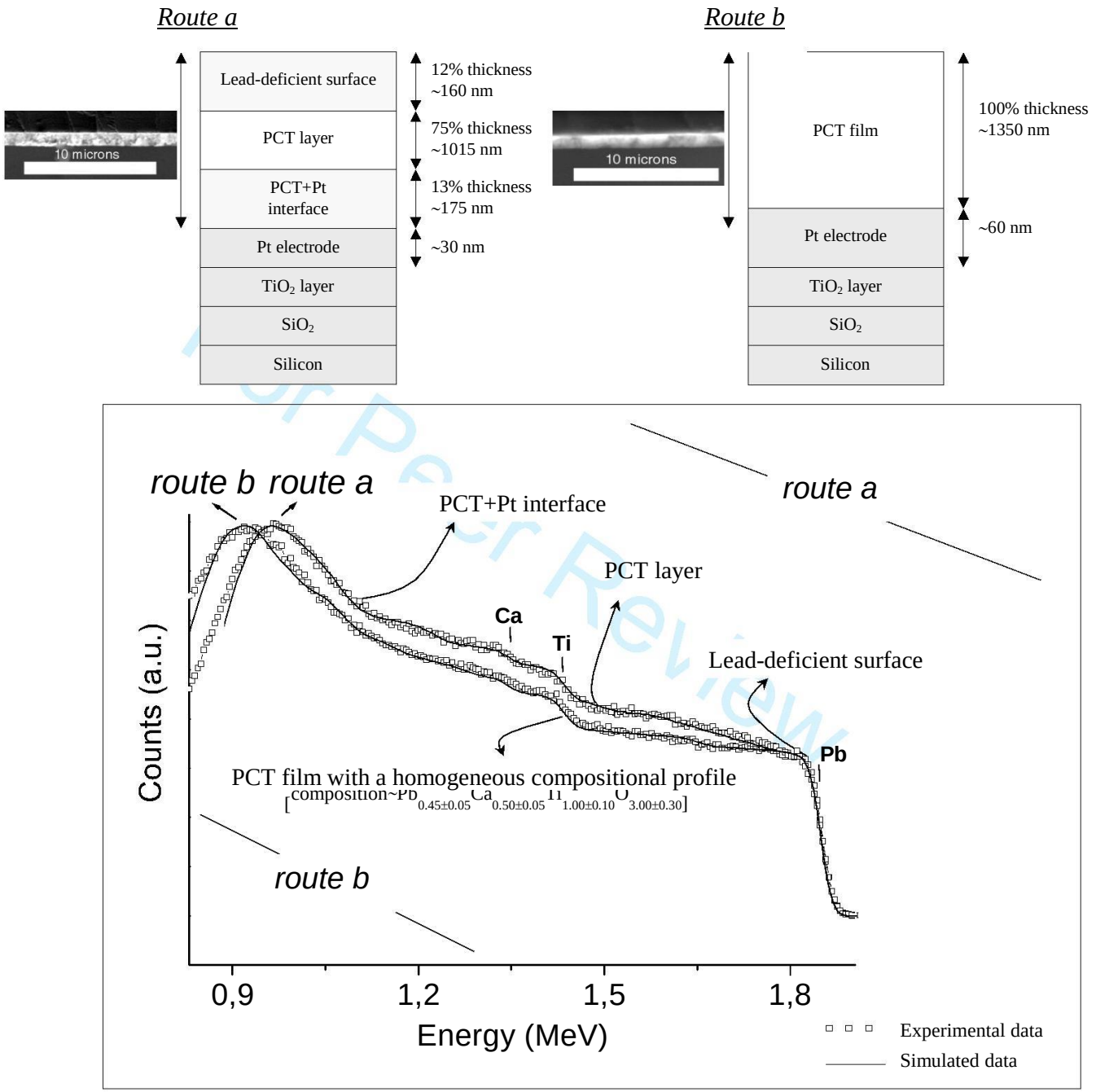

Figure 6

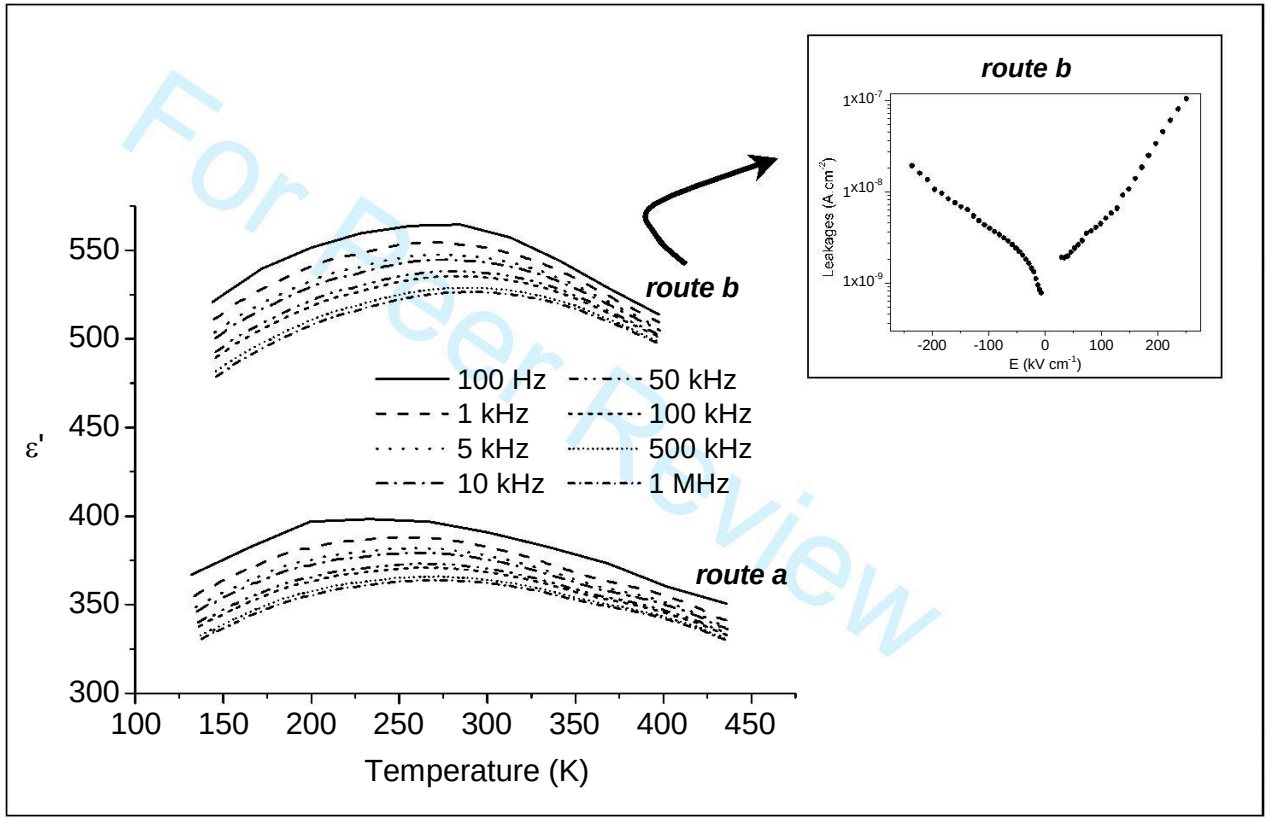

Figure 7

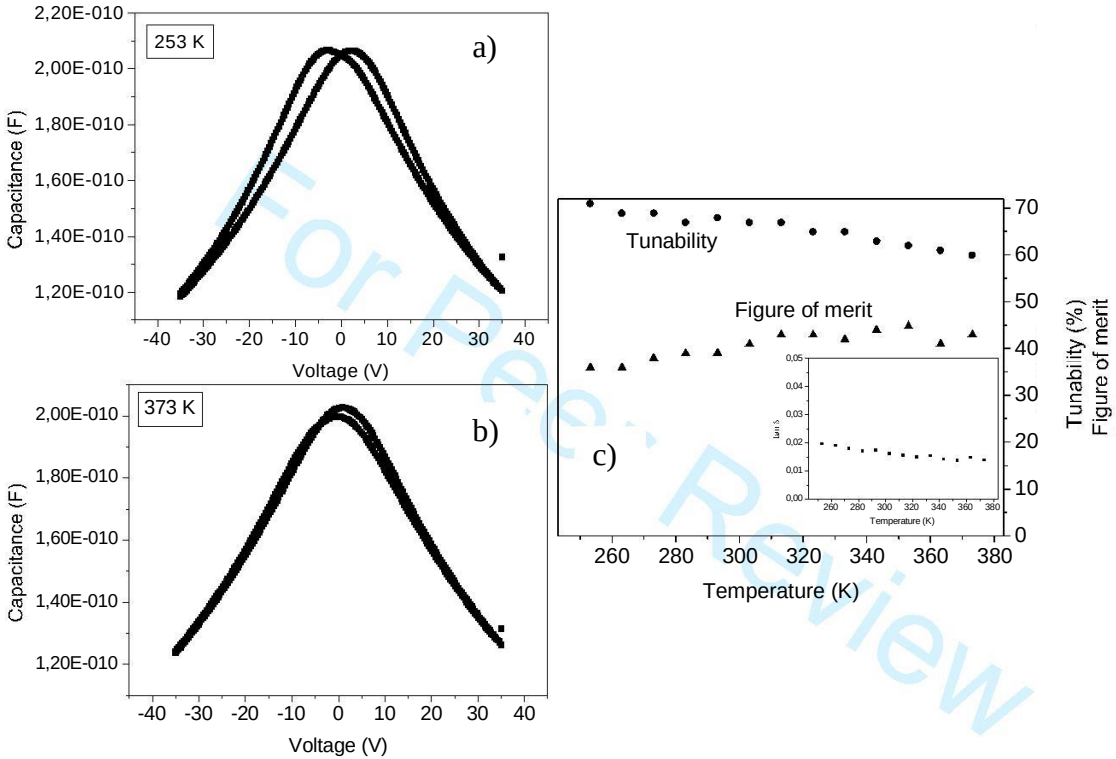

Figure 8